# Enhanced Electrocatalytic Selective CO2-to-CO reduction by a Rhenium(I) complex bearing 6,6′-substituted-2,2′-Bipyridines

| | |
|---|---|
| Journal: | *ACS Catalysis* |
| Manuscript ID | cs-2025-06871b |
| Manuscript Type: | Article |
| Date Submitted by the Author: | 26-Sep-2025 |
| Complete List of Authors: | Abudayyeh, Abdullah; Université catholique de Louvain, Institute of Condensed Matter and Nanosciences (IMCN)<br>De Kreijger, Simon ; Universite catholique de Louvain, Institute of Condensed Matter and Nanosciences<br>Grau, Sergi; The Barcelona Institute of Science and Technology, Inst of Chem. Res. of Catalonia (ICIQ)<br>Eryılmaz, Eren; Gebze Technical University Faculty of Science, Chemistry<br>Robeyns, Koen; Universite catholique de Louvain, Institute of Condensed Matter and Nanosciences (IMCN)<br>Ertem, Mehmed; Brookhaven National Laboratory, Chemistry<br>Llobet, Antoni; The Barcelona Institute of Science and Technology, Inst of Chem. Res. of Catalonia (ICIQ)<br>Elias, Benjamin; Universite catholique de Louvain, Institute of Condensed Matter and Nanosciences<br>Troian-Gautier, Ludovic; Université catholique de Louvain, Institute of Condensed Matter and Nanosciences (IMCN) Molecular Chemistry, Materials and Catalysis Division (MOST) |
| | |

# Enhanced Electrocatalytic Selective $CO_2$-to-CO reduction by a Rhenium(I) complex bearing 6,6'-substituted-2,2'-Bipyridines

Abdullah M. Abudayyeh,[a],* Simon De Kreijger,[a] Sergi Grau,[b] Eren Eryılmaz,[c] Koen Robeyns,[a] Mehmed Z. Ertem,[d] Antoni Llobet,[b] Benjamin Elias,[a] Ludovic Troian-Gautier[a], [e] *

[a] Institut de la Matière Condensée et des Nanosciences (IMCN), Molecular Chemistry, Materials and Catalysis (MOST), Université catholique de Louvain (UCLouvain),Place Louis Pasteur 1 box L4.01.02, B-1348 Louvain-la-Neuve, Belgium

[b] Institute of Chemical Research of Catalonia (ICIQ), Av. Països Catalans 16, Tarragona 43007, Spain

[c] Gebze Technical University, Faculty of Science, Chemistry Department, 41400, Gebze/KOCAELI, Turkey

[d] Chemistry Division, Brookhaven National Laboratory, Upton, New York 11973-5000, United States

[e] Wel Research Institute, Avenue Pasteur 6, 1300 Wavre, Belgium

*KEYWORDS. Rhenium • Catalysis • Carbon Dioxide • Electrochemistry*

**ABSTRACT:** The electrochemical reduction of $CO_2$ ($CO_2$RR) into value-added chemicals offers a promising route toward a circular carbon economy and reduced reliance on fossil fuels. A detailed understanding of the structural and electronic factors governing the performance of molecular $CO_2$RR electrocatalysts is essential for the design of efficient, tunable systems. Here, we report a series of rhenium(I) complexes, fac-[$Re^I$(6,6′-(R)$_2$-bpy)(CO)$_3$Cl] (bpy = 2,2′-bipyridine; R = mesityl (mes), 2,4,6-triisopropylphenyl (trip), or isophthalic acid (phth)) and evaluate their electrocatalytic activity. Among these, fac-[$Re^I$(6,6′-(mes)$_2$-bpy)(CO)$_3$Cl] exhibited the highest performance, enabling selective $CO_2$-to-CO conversion for 1 hour with Faradaic efficiency (FE) > 97%, representing an unprecedented activity level for a Re-bpy catalysts. Single-crystal X-ray diffraction and density functional theory (DFT) calculations indicated that favorable $CO_2$ binding could be promoted by the tilting of the 6,6′-(mes)$_2$-bpy ligand, providing mechanistic insight into the observed enhancement. The study consequently demonstrates a rational correlation between the $CO_2$ electrocatalytic performance of Re-bpy catalysts and their structural variations, as derived from X-ray data and corroborated by computational modeling.

While $CO_2$ is an essential component of the dark cycle of some photosynthetic systems, the recent dramatic rise in $CO_2$ atmospheric levels can no longer be compensated by photosynthetic systems or other living organisms, leading to the known consequence of climate change.[1-2] To this end, one mitigation strategy for increasing $CO_2$ levels is to convert it into value-added feedstock, such as CO, $CH_4$ or other branched aliphatic derivatives, which require chemically catalyzed processes. Some possible $CO_2$ reduction products and the corresponding standard redox potentials in aqueous solution (E° / V vs. SHE) are summarized in Eq. 1–5.[3-4] Note that the thermodynamics of these transformations, including the proton reduction reaction (Eq. 6), are very similar, and are thus difficult to differentiate solely based on thermodynamic considerations. As hydrogen will systematically represent a competitive pathway to $CO_2$ reduction catalysis, product analysis is always key to evaluate the catalytic performances.

$$CO_2 + 2H^+ + 2e^- \rightarrow CO_{(g)} + H_2O_{(l)} \quad -0.11\,V\ (Eq.1)$$

$$CO_2 + 2H^+ + 2e^- \rightarrow HCOOH_{(l)} \quad -0.25\,V\ (Eq.2)$$

$$CO_2 + 6H^+ + 6e^- \rightarrow CH_3OH_{(l)} + H_2O_{(l)} \quad +0.02\,V\ (Eq.3)$$

$$CO_2 + 8H^+ + 8e^- \rightarrow CH_{4_{(g)}} + 2H_2O_{(l)} \quad +0.17\,V\ (Eq.4)$$

$$2CO_2 + 12H^+ + 12e^- \rightarrow CH_2CH_{2(g)} + 4H_2O_{(l)} \quad +0.06\,V\ (Eq.5)$$

$$2H^+ + 2e^- \rightarrow H_{2(g)} \quad 0.00\,V\ (Eq.6)$$

Molecular electrocatalysts for $CO_2$ reduction such as rhenium 2,2′-bipyridine derivatives,[5-6] iron porphyrins,[7-8] cobalt and nickel phthalocyanine[9-11] or copper polypyridines[12] have received increased interest due to their high activity, selectivity and tunable electrochemistry through judicious ligand design. These catalysts are well-known to offer high selectivity for the reduction of $CO_2$ to CO in homogeneous phase by a two-electron process. In the early eighties, Lehn and coworkers reported the rhenium(I) tricarbonyl 2,2′-bipyridine complex, *fac*-[$Re^I$(bpy)(CO)$_3$Cl] (**1**) that was active as a homogeneous catalyst for the reduction of $CO_2$ to CO under photo- and electrocatalytic conditions.[5-6] Since then, a plethora of [$Re^I$(bpy)(CO)$_3$Cl] derivatives have been developed and this category of homogeneous catalysts for the $CO_2$ to CO reduction is amongst the most prevalent. The effect of the 2,2′-bipyridine substituents on the electrocatalytic activity has also been studied.[13-15] In addition, with the development of molecular photoelectrodes, [$Re^I$(bpy)(CO)$_3$Cl]-type catalysts have attracted sparking interest for surfaces functionalization,[16] including enhanced photocatalytic activity on $TiO_2$ reported by Reisner and coworkers,[17] or on $Cu_2O$ as photocathode for $CO_2$ reduction reported by Grätzel, Mayer and coworkers,[18] and more recently, in quantum dot-sensitized NiO photocathode for electrochemical $CO_2$ reduction by the group of Tian[19] or on silicon substrates.[20-21]

Substituent effects on [$Re^I$(bpy)(CO)$_3$Cl] catalysts have been extensively explored to modulate the $CO_2$ reduction activity. In 2010, Kubiak and coworkers investigated electron-donating and -withdrawing groups at the 4,4′-positions of 2,2′-bipyridine (**Figure 1**, Re-a) and found that 4,4′-di-*tert*-butyl substitution enhanced electrocatalytic $CO_2$-to-CO conversion, achieving a second-order rate constant of 1000 $M^{-1}s^{-1}$.[13] Similarly, Müller, Polo, and colleagues varied 4,4′-substituents to assess their photocatalytic $CO_2$ reduction reaction ($CO_2$RR) activity (**Figure 1**, Re-b).[22] Complexes bearing electron-donating groups (–$CH_3$, –$OCH_3$) exhibited slower excited-state quenching with sacrificial donors such as BIH and TEOA compared to electron-withdrawing groups (–Br, –COOH, –$CO_2CH_3$). However, the former reacted more rapidly with $CO_2$ upon one-electron reduction, underscoring the trade-off between photophysical and chemical steps.

Costentin, Chardon-Noblat, and co-workers examined 5,5′-substituted bpy ligands (**Figure 1**, Re-c,d) and showed that conjugated carboxylic or

non-conjugated phosphonate esters diminished the activity via electron-withdrawing effects.[14] In general, such groups lower the overpotential (η) but reduce turnover frequency (TOF), whereas electron-rich substituents enhance TOF at the expense of increased η.

To overcome this trade-off, functionalization in the second coordination sphere (SCS) has emerged as a powerful strategy, with precedents in biomimetic chemistry,[23-24] hydrogen evolution,[25] and $O_2$ evolution catalysis.[26] In $CO_2$RR, SCS modifications in Fe–tetraphenylporphyrins, such as pendant trimethylanilinium, enhance activity via through-space electrostatic effects.[27-28] Similar concepts have been applied to Re catalysts,[29-36] including installation of local proton sources,[32-33] intramolecular hydrogen-bond donors,[34] and ionic groups proximal to the active site[35] to stabilize the metal–carboxylate intermediate.

For [Re$^{I}$(bpy)(CO)$_3$Cl] (1), the 6,6′-positions offer close proximity to the Re center and are ideal for SCS functionalization. In 2017, Nippe *et al.* introduced a redox-active imidazolium group (**Figure 1**, Re-e), which shifted the onset potential 100–150 mV positive relative to **1** and improved the corresponding activity.[31] Incorporation of a phenyl-2,6-diol moiety (**Figure 1**, Re-f) as a local proton source enabled catalysis after the first reduction wave, achieving a TON of 14.1 at –1.7 V vs. Ag|AgCl in MeCN/$H_2O$ (5%).[32] Jurss and co-workers installed pendant aniline groups (**Figure 1**, Re-g) in *ortho*-, *meta*-, or *para* positions, finding that the meta-substituted complex exhibited the highest TOF (239 $s^{-1}$) and a Faradaic efficiency (FE) of 89% in MeCN/4% TFE.[34] Lewis base groups in the SCS (**Figure 1**, Re-h) have also been shown to orient Brønsted acids, enhancing FE to 84% and achieving TON = 14.[36] Matsubara and co-workers combined hydroxy and trimethylammonium substituents (**Figure 1**, Re-i) to couple proton delivery with Coulombic stabilization, lowering the overpotential in DMF/$H_2O$.[28] Marinescu and colleagues further probed pendant amines (**Figure 1**, Re-j) at the 6,6′-positions, finding that $NH_2$ groups increased FE with applied potential, reaching 83%, whereas $NMe_2$ analogues displayed moderate, potential-independent FE (41–65%).[35]

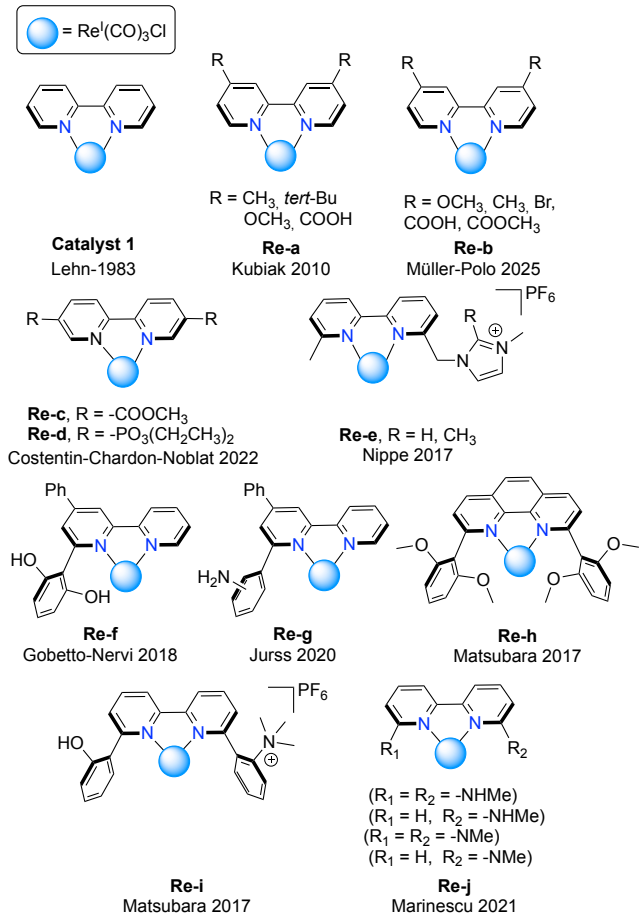


Figure 1. Chemical structure of selected examples of Re-based complexes used for $CO_2$ to CO electrocatalytic reduction.

Collectively, these studies establish that SCS engineering can modulate redox properties, overpotentials, and $CO_2$ binding kinetics in Re–bpy catalysts, offering multiple levers to enhance activity and selectivity. Here, we target this site with sterically demanding aromatic substituents (**Figure 2**) to simultaneously tune electronic structure, suppress dimerization, and probe SCS effects on product selectivity and intermediate stabilization. We prepared mesityl (mes, **2**: [Re$^{I}$(bpy$^{mes}$)(CO)$_3$Cl]), 2,4,6-triisopropylphenyl (trip, **3**: [Re$^{I}$(bpy$^{trip}$)(CO)$_3$Cl]), and isophthalic acid (phth, **4**: [Re$^{I}$(bpy$^{phth}$)(CO)$_3$Cl]) derivatives and evaluated their electrocatalytic $CO_2$RR performance in the absence and presence of weak proton sources (methanol, phenol, and 2,2,2-trifluoroethanol), benchmarking against the prototypical [Re$^{I}$(bpy)(CO)$_3$Cl] (**1**) and rationalizing the difference in electrocatalytic performance via comprehensive density functional theory (DFT) computational studies.

## Results and Discussion

**Synthesis.** The desired 6,6′-(Br)$_2$-2,2′-bipyridine ligand was obtained through the copper-assisted homo-coupling of 2,6-dibromo-pyridine. Afterwards, two types of substituents were coupled through a typical Suzuki coupling reaction (**Figure 2**). Coupling to electron-rich substituents, namely 2,4,6-trimethylphenyl (mes) and 2,4,6-triisopropylphenyl (trip) gave rise to the two corresponding 6,6′-functionalized 2,2′-bipyridine ligands, i.e. bpy$^{mes}$ and bpy$^{trip}$, respectively. Coupling to the electron-poor isophthalic acid derivative gave rise to the corresponding bpy$^{phth}$ ligand. The Suzuki coupling took place at reflux in toluene/methanol mixture in the case of bpy$^{mes}$ and bpy$^{trip}$, and in a methanol/water mixture in the case of bpy$^{phth}$. The corresponding 6,6′-(R)$_2$-2,2′-bipyridine were isolated in moderate to excellent yield (56-94%). The formation and purity of these ligands was confirmed by $^{1}$H NMR, $^{13}$C NMR and high-resolution mass spectrometry.

The four targeted complexes (**1-4**, **Figures 1** and **2**) were prepared in yields greater than 60 % by reacting one equivalent of the appropriate ligand (bpy, bpy$^{mes}$, bpy$^{trip}$ and bpy$^{phth}$) with one equivalent of [Re$^{I}$(CO)$_5$Cl]. In the case of complexes **1-3**, the reaction proceeded smoothly in refluxing toluene for 24 hours, whereas complex **4** required extensive heating in methanol for four days as the solubility of the bpy$^{phth}$ prevented carrying out the reaction in toluene. The extended reaction time most probably originated from the increased bulkiness of this ligand, disfavoring access to the chelation site. Complexes **1–3** are soluble in most common solvents: they are highly soluble in acetone, acetonitrile and dimethylformamide (DMF), and have moderate solubility in dichloromethane and chloroform but show poor solubility in water. Complex **4** bearing the isophthalic moiety is only soluble in DMF and DMSO and sparingly soluble in acetonitrile. The complexes were characterized by $^{1}$H and $^{13}$C NMR, high-resolution mass spectrometry (HRMS), UV-vis absorption, steady-state and time-resolved photoluminescence spectroscopy along with electrochemical measurements. In addition, single crystals suitable for X-Ray diffraction were obtained for complexes **2** and **3** by the slow diffusion of hexane into a chloroform solution of the complexes, while crystals of **4** were obtained by slow diffusion of diethyl ether into a methanolic solution of **4** (**Figure 3**). The XRD structure revealed a 6-coordinate geometry for the Re(I) center with three CO groups occupying one face of the octahedral (*fac*) and the chloride occupying the axial position. Varying degrees of tilting between the bipyridine plane and the Re-CO coordination plane were observed (**Figure 3**, bottom).[37] Complexes **2** and **4** exhibited the largest tilt angle of 23.53° and 21.28°, respectively, while complex **3** displayed a significantly low tilt angle of 7.20°.

**Photophysical properties.** UV-vis absorption and photoluminescence spectra of complexes **1-4** were recorded in argon purged DMF and are all displayed in the supporting information (**Figure S18**). The complexes displayed the typical metal-to-ligand charge transfer (MLCT) transitions around 370-380 nm.[38-39] Ligand-based transition are also observed at wavelength below 310 nm. These absorption features and corresponding molar absorption coefficients are gathered in **Table 1**.

The introduction of substituents in the 6,6′ positions of the 2,2′-bipyridine had only marginal effects on the ground-state absorption properties, as complexes **2-4** exhibited similar absorption features and molar absorption coefficients as complex **1**.[22, 40] When irradiated around 375±5 nm, complexes **1-3** exhibited steady-state photoluminescence with maxima that are centered between 630 and 640 nm, in agreement with the literature value of 642 nm reported for complex **1** in dichloromethane.[41-42] Complex **4** exhibited a marked blue-shift of the photoluminescence, with a maximum centered at 607 nm in DMF (**Figure S18**). The excited state of complex **1** decayed mono-exponentially in argon purged DMF with a corresponding excited-state lifetime of 28 ns, once again consistent with the reported value of 39 ns in dichloromethane.[41] The three other complexes exhibited slightly shorter excited-state lifetime, that ranged from 10 to 15 ns.

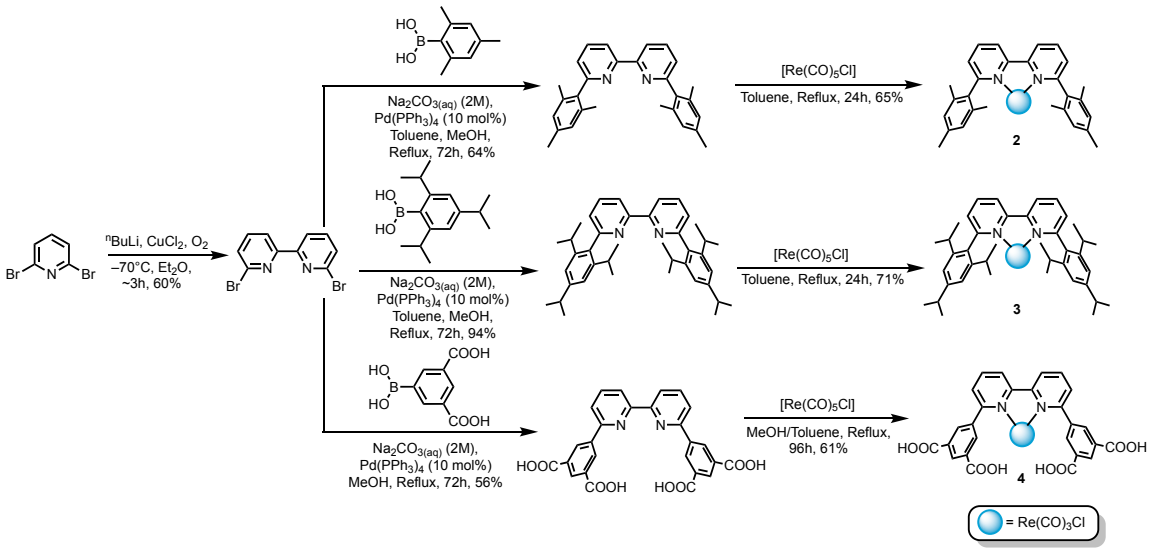


Figure 2. Reaction scheme for the synthesis of the desired 6,6′-bis-aryl-substituted 2,2′-bipyridine ligands and the corresponding complexes.

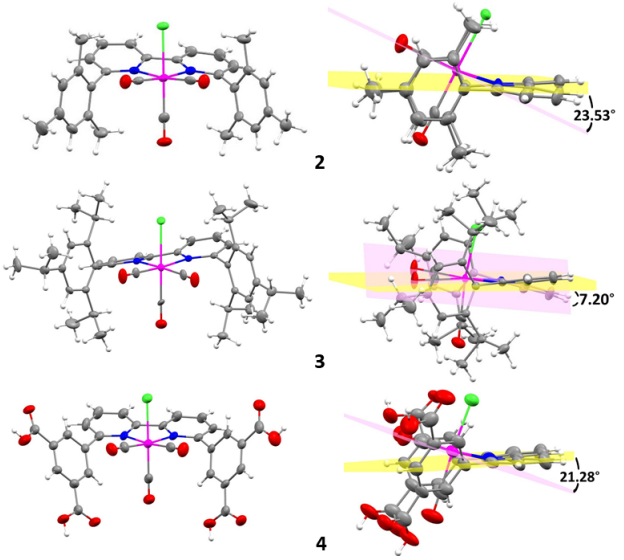


Figure 3. Ortep representation of complexes 2-4 with the front view (left) and side view (right) with ellipsoids shown at the 50% probability level. Solvent molecules were omitted for clarity. The intersecting planes of the bpy (yellow) and Re-CO (pink) display tilt angles of 23.53°, 7.20° and 21.28° for **2**, **3** and **4**, respectively. Color code; rhenium (magenta), nitrogen (blue), oxygen (red) and chloride (green).

**Table 1. Photophysical properties of complexes 1-4 recorded at 20 °C in argon-purged DMF.**

| Re | λ(ϵ)/nm($10^3$ $M^{-1}$ $cm^{-1}$) | $\lambda_{ex}$/ nm | $\lambda_{em}$/ nm | $\tau_0$/ns |
|---|---|---|---|---|
| **1** | 318 (7.1), 372 (3.1) | 370 | 631 | 28 |
| **2** | 317, 15.3 333 (12.9), 372 (3.0) | 370 | 643 | 10 |
| **3** | 320 (9.6), 336 (7.2), 380 (1.45) | 380 | 645 | 15 |
| **4** | 322 (10.5), 336 (8.9), 378 (1.8) | 380 | 607 | 11 |

**Electrochemistry and electrocatalytic $CO_2$ reduction.** Cyclic voltammetry (CV) experiments of complexes **1-4** were carried out using a 1 mM concentration of complex dissolved in dry DMF in the presence of 0.1 M $Bu_4NPF_6$ supporting electrolyte. The three electrodes setup consisted of a glassy carbon working electrode, a platinum counter electrode and an Ag|AgCl reference electrode. DMF was chosen as solvent in these experiments as it allowed to fully solubilize the four complexes, allowing fair comparison between the redox potentials and electrocatalytic activity of these complexes in identical conditions. The oxidation window comprised two oxidation events. For complex **1**, the first oxidation was irreversible and assigned to the metal-centered $Re^{II/I}$ oxidation resulting in the loss of $Cl^-$ which is then oxidized at more positive potential.[43] Notably, the reversibility of the first oxidation event is enhanced for complexes **2-4**, as evidenced from the variable scan rate cyclic voltammetry (**Figures S19-S22**). Thus, this oxidation event changed from irreversible for **1** to quasi-reversible for **2** and **3** possessing the hydrophobic units and then becomes fully reversible for complex **4** with the isophthalic unit in its SCS (**Figure S22**). Complexes **1-4** exhibited a reversible one-electron reduction wave followed by a second irreversible wave (**Figure 4** and **Table 2**), which are ascribed to ligand-centered reduction followed by an irreversible $Re^{I/0}$ reduction.[6, 44-45] The first reduction occurred at $E_{1/2} = -1.30$ V for the parent complex **1**. This reduction event was slightly shifted to more negative values upon the introduction of electron donating units, i.e. –1.38 V and –1.31 V for complexes **2** and **3**, respectively. Similarly, the introduction of electron-withdrawing units slightly shifted the potential of the first reduction event to more positive potentials for complex **4**, i.e. –1.21 V. Thus, the difference between the first reduction potential of complex **2** and **4** is around 170 mV. It is important to note that the reduction event of complex **4** becomes broad and difficult to observe when the cathodic window is recorded after the anodic scan (**Figure 4**, cyan dashed line). Conversely, when the cathodic scan is recorded first up to –1.50 V and using freshly polished electrode (**Figure 4**, blue trace) the first reduction wave becomes discernible and reversible. This observation highlights the potential for chemical change upon oxidation and potential deposition on the electrode, presumably via oxidative decarboxylation.[46]

**Table 2. Electrochemical properties of complexes 1-4.[a]**

| Re | $E_c$/V ($Re^{I/0}$) | $E_{1/2}$/V ($Py^{0/\bullet-}$) | $E_a$/V ($Re^{II/I}$) | $E_a$/V ($L^{0/\bullet+}$) | (D)/$cm^2$ $s^{-1}$ |
|---|---|---|---|---|---|
| **1** | –1.68 | –1.30 | 1.44 | 1.84 | 4.8 x$10^{-5}$ |
| **2** | –1.91 | –1.38 | 1.38 | 2.00 | 1.7 x$10^{-6}$ |
| **3** | –1.96 | –1.31 | 1.53 | 2.00 | 3.5 x$10^{-6}$ |
| **4** | –1.70 | –1.21c | 1.55 | 2.00 | 1.4 x$10^{-5}$ |

[a]recorded in DMF with 0.1 M $(Bu_4N)PF_6$ supporting electrolyte, scan rate 100 m V/s, glassy carbon working electrode (d = 2 mm, A = 0.03 $cm^2$) vs. Ag|AgCl reference electrode and Pt counter electrode at 20 °C. In this system $E_{1/2}(Fc^+/Fc) = 0.45 \pm 0.01$ V. $E_c$: potential of cathodic wave, $E_a$: potential of anodic wave, $E_{1/2}$ half-wave potential of reversible event.

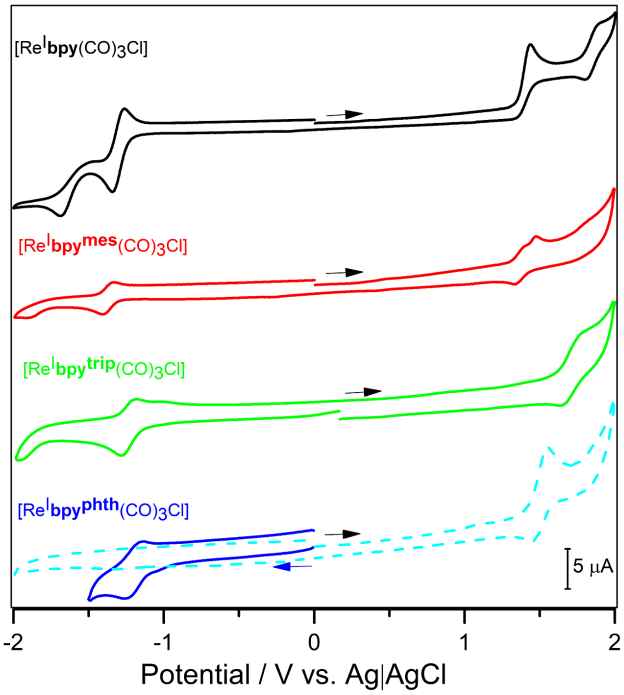


Figure 4. Cyclic voltammetry of $[Re^{I}(bpy)(CO)_3Cl]$ **1** (black), $[Re^{I}(bpy^{mes})(CO)_3Cl]$ **2** (red), $[Re^{I}(bpy^{trip})(CO)_3Cl]$ **3** (green), and $[Re^{I}(bpy^{phth})(CO)_3Cl]$ **4** sweeping (blue) 0.0 V → –1.50 V → 0 and (cyan) 0.0 V → 2.0 V → –2.0 → 0. All experiments were carried out at a concentration of 1 mM of complex in DMF and under argon. Reduction potentials are summarized in **Table 2**. Conditions: 0.1 M $(Bu_4N)PF_6$ supporting electrolyte, scan rate 100 m V/s, glassy carbon working electrode (d = 2 mm, A = 0.03 $cm^2$) vs. Ag|AgCl references electrode and Pt counter electrode at 20 °C. In this system $E_{1/2}(Fc^+/Fc) = 0.45 \pm 0.01$ V.

Plots of the current *vs*. the square root of the scan rate for the first reduction event in complexes **1**-**4** (**Figure S23**) confirmed that this step is reversible and diffusion controlled for the four complexes. This facilitates the use of the Randles-Ševčík equation (see SI) that yielded the corresponding diffusion coefficient ($D$, $cm^2\ s^{-1}$) for each complex.[46-47] Using this equation, diffusion coefficients of 4.8 x $10^{-5}$, 1.7 x $10^{-6}$, 3.5 x $10^{-6}$ and 1.4 x $10^{-5}$ $cm^2\ s^{-1}$ were determined for complexes **1** through **4**, respectively (**Table 2**). For complexes **2** and **3**, the trend in diffusion coefficient is consistent with the fact that the bulky hydrophobic groups slow down the diffusion rate by one order of magnitude compared to **1**. Complex **4**, bearing the hydrophilic isophthalic acid units, diffuses three times slower than the parent complex but still faster than complexes **2** and **3**. This probably stems from the fact that complex **4** is only disubstituted on each phenyl ring whereas complexes **2** and **3** bear trisubstituted derivatives. These diffusion coefficients are in the same range of analogous mono-aryl substituted rhenium-bpy complexes (**Re-g**, **Figure 1**, D = 1.3 x $10^{-5}$ – 1.72 x $10^{-5}$ $cm^2s^{-1}$) reported recently by Jurss and coworkers[34] as well as in close range to the one reported by Dempsey and coworker for ferrocene, i.e. 2.7 $10^{-5}$ $cm^2\ s^{-1}$ in MeCN.[34]

Next, the four complexes were tested as electrocatalysts for $CO_2$ reduction using $CO_2$ saturated DMF in the presence and absence of proton source. Since the first report of Hawecker, Lehn, and Ziessel in 1984,[6] where enhancement in catalytic current was observed when 10% of water was added to a DMF solution of catalyst **1**, the $CO_2$ electrocatalytic enhancement due to the addition of proton sources became well documented in the literature.[7, 44, 48] In here, three proton sources of varying strength were used, i.e. 2,2,2-trifluoroethanol (TFE), methanol (MeOH), and phenol (PhOH) with reported p$K_a$ range of 23.5 to 29.0 in DMSO.[49] Values in DMF were not available in the literature. MeOH as a poor acidic proton source has recently been employed in $CO_2$ electroreduction.[50-51] The use of different proton sources provides insight into the $CO_2$ electrocatalytic performance in terms of stability, activity, and overpotential.

To assess the catalytic efficiency of these novel catalysts, cyclic voltammetry was first recorded for each catalyst under saturated $CO_2$ conditions in the absence of a proton source. For all catalysts, current enhancement was observed at the onset of the second reduction potential (**Figure 5**) with the stark exception of catalyst **2** where a slight catalytic current is observed at the first catalytic wave (*vide infra*). Owing to the irreversibility of the second reduction event under argon atmosphere, the catalytic potential of each catalyst was determined from the value of the potential at midpoint of the catalytic current ($E_{cat/2}$, **Table 3**, ESI-Section 6), which lies in the steepest portion of the catalytic wave.[52] The variation in the value of potential at $E_{cat/2}$ is smaller than that determined from the peak current ($i_{cat}$). This enables to determine the overpotential from the difference between $E_{cat/2}$ and $E°_{CO2/CO}$ in DMF.

An $E_{cat/2}$ of –1.68 V was determined for catalyst **1** in $CO_2$ saturated conditions in the absence of any proton source (**Figure 5** and **Figure S24**) whereas catalysts **2** and **3** have the corresponding $E_{cat/2}$ value negatively shifted by 60 mV and 200 mV, respectively (**Table 3**, **Figure 5** and **Figures S25-S26**). This observation was expected as the electron-donating Mes and Trip substituents render the corresponding catalysts more difficult to reduce, as discussed earlier. Interestingly, catalyst **4**, with its isophthalic acid group, shifted the $CO_2$ reduction event 140 mV more positive than the reference catalyst ($E_{cat/2}$ = –1.54 V for **4** vs. –1.68 for **1**). Although complex **4** initially appeared to exhibit catalytic activity after the first reduction, similar to catalyst **2**, further controlled potential electrolysis (CPE) experiments revealed that its activity was short-lived in the presence of MeOH as the proton source (see below).

The performance of an electrocatalyst for $CO_2$ reduction is evaluated by comparing the peak current of the catalytic wave in presence of $CO_2$ ($i_{cat}$) with the current value of the same event but in the absence of $CO_2$ (under argon, $i_p$). In case of an efficient catalyst, rapid conversion due to high turnover of $CO_2$ by the catalyst can result in a high value of $i_{cat}$ compared to $i_p$ ($i_{cat}/i_p$).[3] For all catalysts, the catalytic activity, dictated by the value of $i_{cat}/i_p$, and the potential at half of the catalytic wave current ($E_{cat/2}$) are both enhanced in the presence of 2,2,2-trifluoroethanol, phenol or methanol (**Table 3, Figures S24-S27**), with the exception of catalyst **4**, for which the catalytic potential is slightly shifted to more negative value with the presence of 3 M PhOH (–1.57 V) and drastically shifted to –1.93 V in the presence of 3 M TFE, likely triggering the proton reduction process. In the absence of proton source, catalyst **2** displayed an $i_{cat}/i_p$ value that is twice that of the other catalysts. This observation is most probably due to residual water in the cell or in the solvent that serves as proton source. Among all proton source used in this study, MeOH produced the most significant positive shift in catalytic potential ($E_{cat/2}$), with catalyst **1**, **2** and **4** exhibiting nearly identical ranges for $E_{cat/2}$ between –1.39 V and –1.46 V. Conversely, catalyst **3** exhibited an $E_{cat/2}$ of –1.59 V in the presence of 6.2 M MeOH. Reference catalyst **1** catalyzed the $CO_2$ reduction in the absence of proton sources at $E_{cat/2}$ of –1.68 V with an $i_{cat}/i_p$ of 3.4, which is in good agreement with the $i_{cat}/i_p$ of 4.4 reported by Nippe and coworkers for the same catalyst in acetonitrile without a proton source.[31] In the presence of 6.2 M MeOH, the $E_{cat/2}$ for this catalyst shifted positively to –1.39 V with an $i_{cat}/i_p$ of 7.7. Compared to **1**, the newly studied catalysts displayed improved $i_{cat}/i_p$ values in the presence of MeOH with the exception of catalyst **4** bearing the isophthalic groups, that showed slightly lower $i_{cat}/i_p$ of 5.7. Remarkably, catalyst **2** featuring the dimesityl group stands out with an $i_{cat}/i_p$ of 21.3, nearly four times greater than that of reference catalyst **1** and double that of catalyst **3** ($i_{cat}/i_p$ of 11.1).

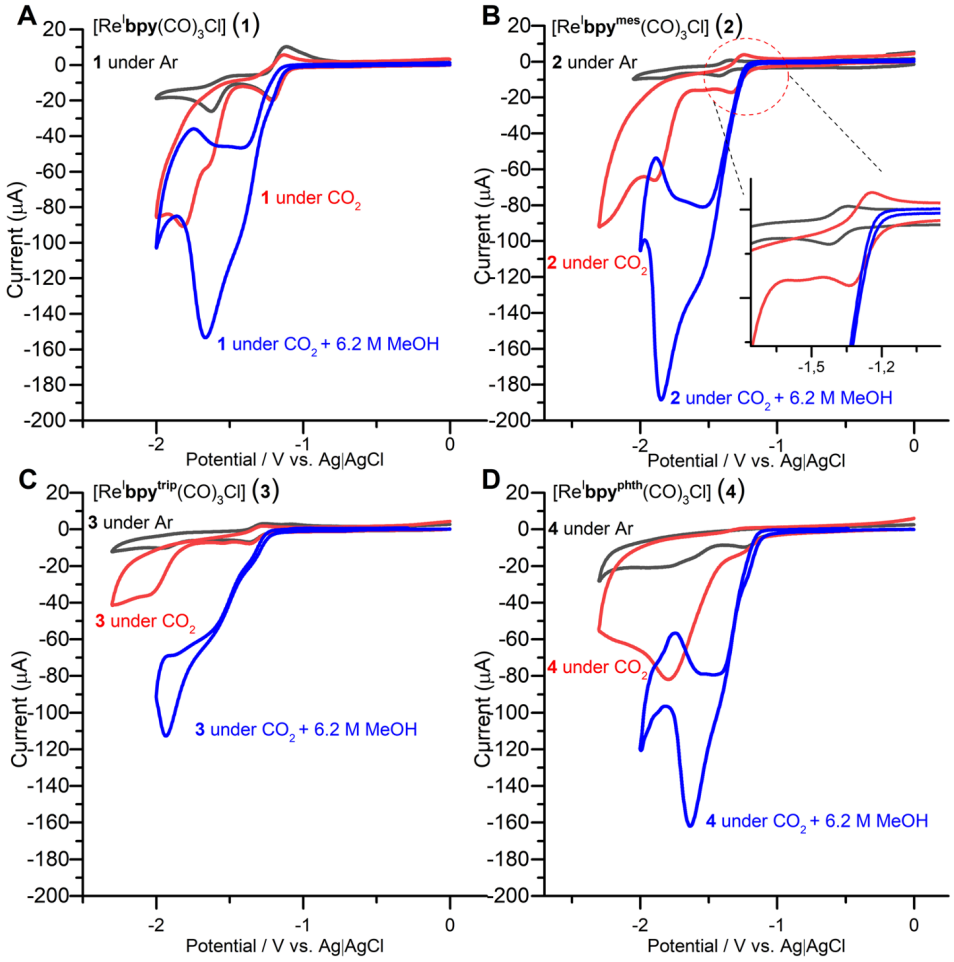


**Figure 5.** Cyclic voltammetry of 1 mM DMF solutions of [Re$^{I}$(bpy)(CO)$_3$Cl] **1** (a), [Re$^{I}$(bpy$^{mes}$)(CO)$_3$Cl] **2** (b), [Re$^{I}$(bpy$^{trip}$)(CO)$_3$Cl] **3** (c), and [Re$^{I}$(bpy$^{phth}$)(CO)$_3$Cl] **4** (d) recorded under Ar (black), $CO_2$ (red) and $CO_2$ in the presence of 6.2 M MeOH (blue). Plots with other proton sources are shown in ESI Section 6 with catalytic performance summarized in **Table 3**. Inset in B shows an enlarged portion of the CV where the pre-catalytic wave is observed near the first reduction event of **2**. Conditions: 0.1 M $(Bu_4N)PF_6$ supporting electrolyte, scan rate 100 mV/s, glassy carbon working electrode (d = 2 mm, A = 0.03 cm$^2$) vs. Ag|AgCl references electrode and Pt counter electrode at 20 °C. In this system $E_{1/2}(Fc^+/Fc) = 0.45 \pm 0.01$ V.

**Table 3. Catalytic performance of catalysts 1-4 under $CO_2$ in DMF in absence and presence of proton source; 2,2,2-trifluoro-ethanol (3 M TFE), phenol (3 M PhOH) and methanol (6.2 M MeOH).**

| | $i_{cat}/i_p$ | | | | $E_{cat/2}$ (V vs Ag\|AgCl) | | | |
|---|---|---|---|---|---|---|---|---|
| **Catalyst** | *No* $H^+$ | TFE | PhOH | MeOH | *No* $H^+$ | TFE | PhOH | MeOH |
| [Re$^{I}$(bpy)(CO)$_3$Cl] **1** | 3.4 | 10 | 10 | 7.7 | –1.68 | –1.51 | –1.58 | –1.39 |
| [Re$^{I}$(bpy$^{mes}$)(CO)$_3$Cl] **2** | 7.6 | 9.2 | 6.2 | 21.3 | –1.74 | –1.59 | –1.69 | –1.46 |
| [Re$^{I}$(bpy$^{trip}$)(CO)$_3$Cl] **3** | 3.4 | 6.7 | 5.2 | 11.1 | –1.88 | –1.67 | –1.80 | –1.59 |
| [Re$^{I}$(bpy$^{phth}$)(CO)$_3$Cl] **4** | 3.9 | 9.2 | 9.0 | 5.7 | –1.54 | –1.93 | –1.57 | –1.36 |

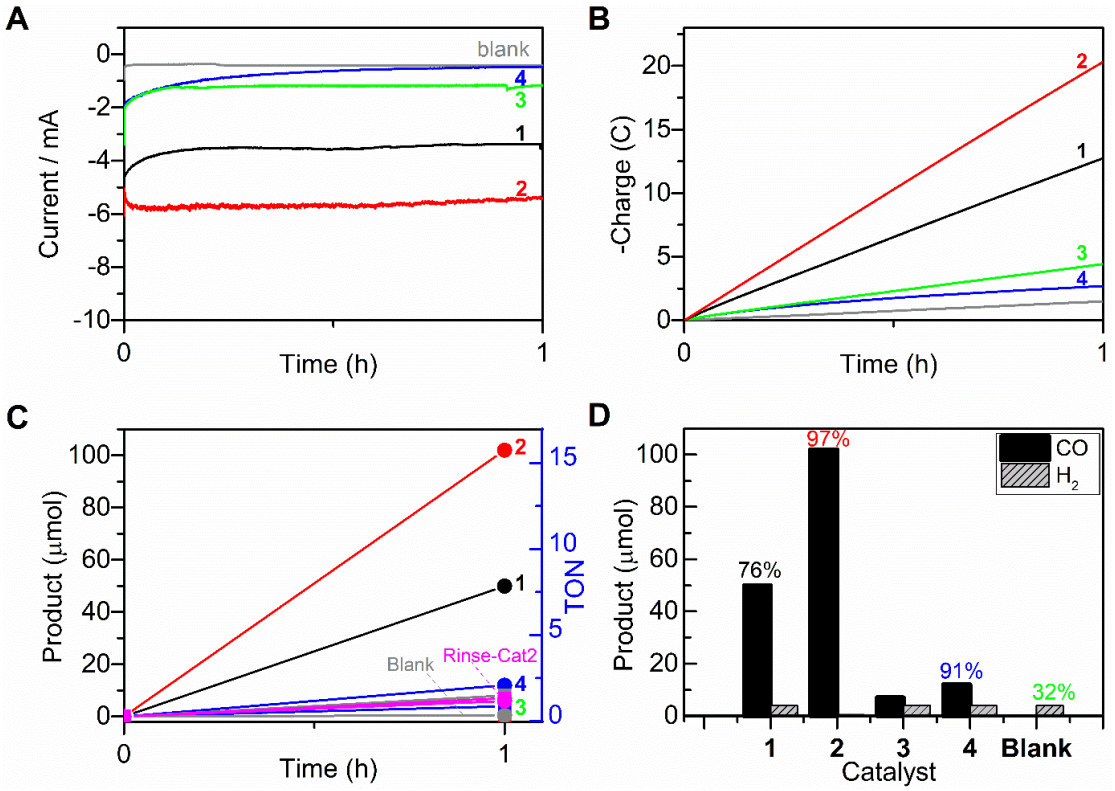


**Figure 6.** Controlled potential electrolysis (CPE) experiment at –1.80 V (vs. Ag|AgCl) of $CO_2$-saturated DMF solutions in the presence of 6.2 M MeOH for the blank (grey), and with 1 mM of catalyst **1** (black), **2** (red), **3** (green) and **4** (blue). (A) Current-time plot for 1 hour CPE experiment, (B) corresponding charge-time plot for the experiment in A. (C) product distribution analysis (circles: CO, squares: H2) from the 1 hour CPE experiment along with the rinse test (magenta) by which the working electrode used with catalyst 2 was gently dipped in DMF and then the electrolysis was repeated in $CO_2$ saturated freshly made electrolyte in the presence of 6.2 M MeOH. (D) Bar chart for the analysis of the gaseous product for CO (black solid bars) and $H_2$ (dashed bars), the CO Faradaic efficiency is indicated on the top of the bar for each catalyst.

To further evaluate the long term electrocatalytic $CO_2$ activity of these catalysts, controlled potential electrolysis experiments were conducted at an applied potential of –1.80 V *vs.* Ag|AgCl using 1 mM of the desired catalyst in DMF with 6.2 M MeOH and a glassy carbon working electrode (A = 3.1 $cm^2$). As illustrated in **Figure 6**, catalysts **1**-**4** exhibited varying performances in $CO_2$ reduction. Catalyst **2** displayed the highest current value over the course of one hour, averaging –5.5 mA. It achieved a total charge of 20.3 C and produced 102 µmol of CO along with a Faradaic efficiency (FE) of 97% and no trace of $H_2$ detected. Rinsing experiments, whereby the electrode was removed after the CPE experiment using catalyst **2** showed minimal activity, with a charge accumulation and gas analysis similar to that recorded for the blank (**Figure 6C**). The unmodified reference complex (**1**) ranked second in reactivity under the same experimental conditions, yielding half the amount of CO (50 µmol) compared to **2**, with a FE of only 76% and trace amounts of $H_2$. The FE of **1** was twice that reported by Nippe for the same catalyst in MeCN with 10% water as the proton source.[31] In contrast to **1** and **2**, catalysts **3** and **4** demonstrated drastically reduced activity for $CO_2$ reduction, resulting in charge accumulation over one hour of 4.5 C for **3** and 2.7 C for **4**. The current density for **4** was also observed to decrease significantly after 30 minutes of electrolysis, indicating a loss of activity. For catalysts **3** and **4**, only a minimal amount of CO was detected (7-11 µmol) and only traces of $H_2$, while no other products dissolved in the liquid phase were detected, thereby confirming their low activity. The significantly reduced catalytic performance of catalyst **4** along with its rapid deactivation is likely due to the electron-withdrawing nature of the carboxylic acid groups attached to the 6,6' positions. These groups likely destabilize the electron-deficient metal center in the metallocarboxylate reaction intermediate ($CO_2H$-$Re^I$), which is crucial for the $CO_2$ reduction reaction.[30-31, 34] In contrast, this intermediate can be stabilized by the electron donating groups, as manifested effectively in catalyst **2**. The same reasoning applies to catalyst **3** with the Trip groups, however, the –1.8 V applied potential may not be significantly advantageous for **3**, as the catalytic wave observed for this catalyst is the most negative among those studied. Additionally, the requirement to apply a potential even more negative than –1.8 V, as used in this study, is not desirable for catalysis. Control experiments in the absence of catalyst demonstrated negligible CO formation over the duration of one hour, with hydrogen being the sole product generated. Altogether, these experiments confirmed that **2** is acting as an efficient homogeneous molecular $CO_2$RR catalyst and highlights that the SCS significantly influences the catalytic performance of the Re-bpy catalyst for $CO_2$ reduction. The modification of the SCS with the electron-donating mesityl group not only increased the catalytic activity but also shifted the potential required for catalysis to better align with the first reduction wave, thereby enhancing the longevity of the resulting catalyst. Conversely, the introduction of either larger electron-donating Trip groups or electron-withdrawing isophthalic groups reduced the activity for $CO_2$ reduction in DMF with MeOH (6.2 M) as the proton source.

**Computational modeling**. To rationalize these observations and gain insight into the activation pathways for $CO_2$ reduction, density functional theory calculations at the MN15 level,[53] in combination with the SMD solvation model[54] for DMF were performed. The computed reaction pathways are represented in **Figure 7**, with the computed values for each step presented in **Table 4**. We started our mechanistic investigation with the first reduction potential of the $[\textbf{Re-Cl}]^0$ or $[\textbf{Re-DMF}]^+$ complexes. The four catalysts, whether bearing Cl or DMF axial ligands exhibit reduction potentials that span a narrow range, i.e. $E_1$ = –1.47 to –1.66 V and $E_4$ = –1.32 to –1.44 V. Following this first reduction event, the catalysts can either undergo ligand loss (Cl or DMF) according to steps $\Delta G_1$ and $\Delta G_2$ or a second reduction with concerted ligand loss as indicated by $E_2$ and $E_5$ in **Figure 7**. Among the catalysts investigated, the catalyst bearing the bulkiest substituent (**3**) exhibited the lowest free energy changes of 5.2 kcal $mol^{-1}$ and –0.7 kcal $mol^{-1}$ for chloride ion and DMF dissociation, respectively. The computed potential for the subsequent reduction of the penta-coordinated $[Re]^0$, resulting in the active two-electron reduced species $[Re]^-$, also lies within a narrow-computed range, i.e. $E_3$ = –1.44 to –1.59 V. Furthermore, the reduction of $[Re\text{-}Cl]^-$ with the concerted loss of $Cl^-$ requires a more negative

potential ($E_2$ = –1.75 to –2.00 V), whereas the reduction of [Re-DMF]$^0$ with the concerted loss of DMF results in a lower energy requirement with computed potentials of $E_5$ = –1.49 to –1.63 V. Thus, at this stage it appears that the formation of the doubly reduced species is thermodynamically feasible for all catalysts, but that the free energy cost and the computed potentials are overall more favorable once the initial chlorido ligand has been replaced by the solvent.

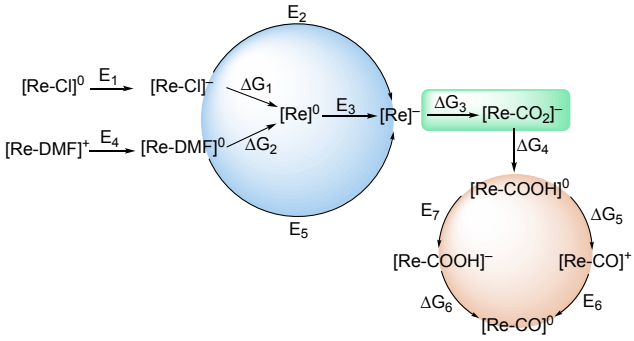


**Figure 7.** Computed activation steps for [Re-Cl]$^0$ and solvated [Re-DMF]$^+$ species.

Interestingly, the computed free energy values for the $CO_2$ binding to the doubly reduced species (**[Re]$^-$**) to form carboxylate intermediates (**[Re-CO$_2$]$^-$**) ($\Delta G_3$ highlighted in green in **Figure 7**) ranges between 7.0 kcal mol$^{-1}$ for the most active catalyst featuring the mesityl-moiety (**2**) to 13.4 kcal mol$^{-1}$ for the least active catalyst featuring the excessively bulky trip-moiety (**3**), thereby indicating a more favorable $CO_2$ binding free energy for catalyst **2**. At first glance, these results could appear counter-intuitive as the mesityl groups are expected to also provide a significant steric hindrance for $CO_2$ binding, especially compared to the parent *fac*-[Re$^I$(bpy)(CO)$_3$Cl] catalyst. Interestingly, a closer look at the computed geometries of the different catalysts indicated that the active catalyst **2** displayed a significant tilting of the 2,2'-bipyridine unit compared to the other catalysts (**Figure 8**), as reported for other active catalysts.[37] This was also confirmed by X-Ray crystallography (**Figure 3**). Specifically, theoretical calculations allowed to determine a tilt angle of 6° for **1**, 20° compared to 23.53° (XRD) for **2**, and 2.5° compared to 7.20° (XRD) for **3**. As $\Delta G_3$ represents the only computed energy where significant differences were observed, it could thus represent a key step within the catalytic cycle and suggests that the bending of **2** may account for the higher activity of this complex in overall $CO_2$ conversion. Additional pathways were also computed, such as the disproportionation of the mono-reduced species, [Re-DMF]$^0$ and [Re-Cl]$^-$. Although thermodynamically feasible, they do not exhibit systematic differences between the catalysts examined in this study.

**Table 4. Summary of computed reduction potentials (E in V vs Fc$^+$/Fc ) and free energy changes (ΔG in kcal mol$^{-1}$) for [Re(6,6'-(R)$_2$-bpy)(CO)$_3$X] pre-catalysts (1-4)**

| Re | $E_1$ | $E_2$ | $E_3$ | $E_4$ | $E_5$ | $E_6$ | $E_7$ | $\Delta G_1$ | $\Delta G_2$ | $\Delta G_3$ | $\Delta G_4$ | $\Delta G_5$ | $\Delta G_6$ |
|---|---|---|---|---|---|---|---|---|---|---|---|---|---|
| **1** | 1.58 | 1.97 | 1.55 | 1.42 | 1.53 | –1.33 | –1.70 | 9.9 | –0.4 | 8.4 | –13.3 | 5.7 | –2.9 |
| **2** | 1.66 | 2.00 | 1.59 | 1.44 | 1.63 | –1.25 | –1.65 | 9.3 | 0.8 | 7.0 | –13.1 | 5.5 | –3.8 |
| **3** | 1.60 | 1.75 | 1.52 | 1.41 | 1.49 | –1.31 | –1.68 | 5.2 | –0.7 | 13.4 | –14.6 | 4.2 | –4.2 |
| **4** | 1.47 | 1.96 | 1.44 | 1.32 | 1.53 | –1.20 | –1.57 | 12.1 | 2.1 | 10.2 | –11.4 | 6.5 | –1.9 |

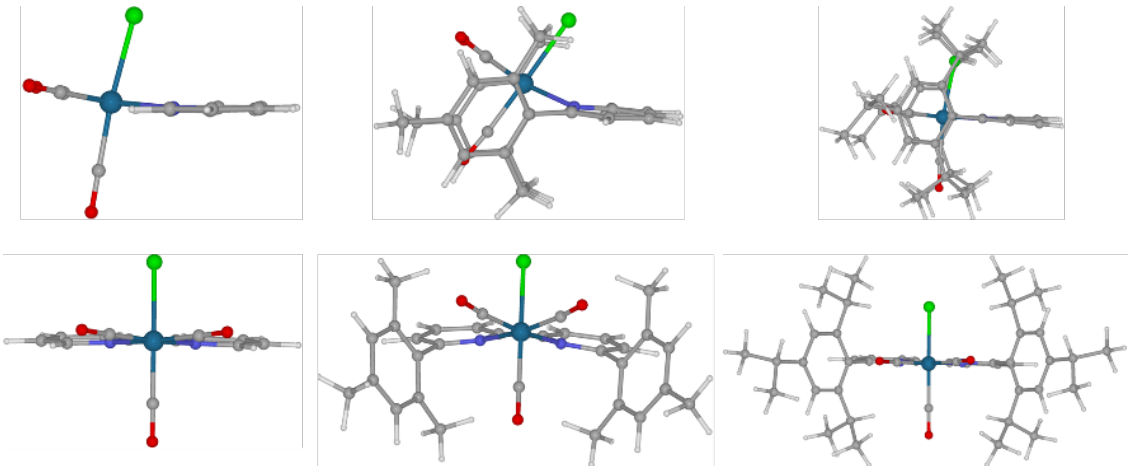

**Figure 8.** Calculated structures for catalysts **1**, **2**, and **3**, from left to right.

## Conclusion

Three 6,6'-substituted 2,2'-bipyridine ligands were synthesized using Suzuki coupling reaction between 6,6'-dibromo-2,2'-bipyridine and the corresponding 2,4,6-trimethylphenyl (Mes), 2,4,6-triisopropylphenyl (Trip) and isophthalic (Phth) boronic acid. These groups vary in their bulkiness and electron donating ability, allowing for fine tuning of fundamental properties. These ligands were used for the synthesis of a series of Re(I) complexes that were evaluated for $CO_2$ reduction and benchmarked against the prototypical [Re$^I$(bpy)(CO)$_3$Cl] catalyst, in the absence and presence of weak Brønsted acids. Although the introduction of bulky mesityl and triisopropylphenyl groups had minor effects on the first reduction event at –1.30 V, the potentials of the second reduction event shifted to more negative values under inert conditions to –1.91 V for **2** and –1.96 V for **3** compared to –1.68 V for **1** and –1.70 for **4**, respectively.-Methanol positively impacted the electrocatalytic activity represented by $i_{cat}/i_p$, following trend in activity where **2** > **3** > **1** > **4** with $i_{cat}/i_p$ = 21.3 > 11.1 > 7.7 > 5.7. CPE experiments conducted at –1.80 V for one hour indicated highest turnover number of 16 achieved by the most active catalyst **2**, followed by the literature structurally unmodified catalyst **1** with TON ~**7**, whereas the least active catalysts **3** and **4** displayed minimal TON ~1.

Experimental and theoretical calculations point towards the tilting of catalyst **2**, in addition to the incorporation of electron donating groups, as key factors controlling the catalysis. Indeed, whereas potentials shifts are well understood based on electronic factors, geometric contributions are currently less rationalized. In the present case, it appears that the tilting of catalyst **2** favors the key insertion of $CO_2$ compared to the other catalysts, which is paramount to initiate the reductive chemistry. This can be the factor rendering catalyst **2** faster and more efficient than **1**, **3**, and **4** and as a consequence, the competing hydrogen formation reaction and/or other

deactivation processes are minimized. This represents an approach that warrants future investigations in the coming future.

**Experimental section**

$^1$H-NMR and $^{13}$C NMR spectra were recorded on a Bruker AC-300 Avance II (300 MHz) or a JEOL JNM-ECZL R (400 MHz and 600 MHz) at 293 K. Chemical shifts are reported in parts per million and referenced to the residual protonated solvent peak in the $^1$H NMR spectra and the residual solvent peak in the $^{13}$C NMR spectra [$CDCl_3$: 7.26 ppm ($^1$H) and 72.16 ppm ($^{13}$C); $d_6$-DMSO: 2.50 ppm ($^1$H) and 39.52 ppm ($^{13}$C)]. High-resolution ESI-MS was performed with a Q-Extractive orbitrap from ThermoFisher using reserpine as the internal standard. Samples were ionized by electrospray ionization (ESI). UV−vis absorption spectra were recorded on an Agilent Cary 60 spectrophotometer in a quartz cuvette with a 1 cm path length. Molar absorption coefficients were determined in at least two independent measurements with less than 5 % standard deviation.

Time-resolved and steady-state photoluminescence spectra were recorded on an FS5 Spectrofluorometer from Edinburgh Instruments equipped with a time-correlated single photon counting module. The steady-state photoluminescence spectra were recorded using a 150 W Xenon arc lamp as the excitation source. The photoluminescence was detected at a right angle to the excitation beam using a single photon counting PMT-900 in a temperature-stabilized housing. The spectra were integrated for 0.1–0.2 s at each wavelength. Time-resolved photoluminescence data were collected on the FS5 spectrofluorometer using the time-correlated single photon counting technique (TCSPC). Excitation was achieved with a 450±5 nm diode laser (EPL-450, 85 ps pulse width at 10 MHz) for rhenium complexes. Photons reaching the detector were accumulated to reach a count of 5,000.

Cyclic voltammetry (CV) was performed with an Autolab PGSTAT 100 potentiostat using a standard three-electrodes cell, i. e., a glassy carbon disk working electrode (d = 2 mm, A = 0.03 $cm^2$), a platinum wire counter electrode and an aqueous Ag|AgCl reference electrode. Experiments were performed in dry DMF with 0.1 M $TBAPF_6$ as supporting electrolyte at a scan rate of 0.1 V/s.

Computational Methods. All geometries were fully optimized at the MN15 level of density functional theory,[53] in conjunction with the SMD continuum solvation model[54] for DMF using the def2-TZVP basis set on Re[55] and the def2-SVP basis set[55] on all other atoms. Non-analytical integrals were evaluated using the integral=(grid=ultrafine) option as implemented in the Gaussian 16 software package.[56] The nature of all stationary points was verified by analytic computation of vibrational frequencies, which were also used for the computation of zero-point vibrational energies and molecular partition functions. Partition functions were used in the computation of 298 K thermal contributions to the free energy employing the usual ideal-gas, rigid-rotator, harmonic oscillator approximation.[57] Free-energy contributions were added to single-point MN15 electronic energies computed using SMD continuum solvation model for DMF at the optimized geometries obtained with the initial basis with def2-TZVPP basis set on Fe and Re and the def2-TZVP basis set on all other atoms to arrive at final composite free energies. The reduction potentials are computed in reference to $Fc^+$/Fc couple.

Single crystal determination was performed on a MAR345 image plate detector using MoKα radiation generated by an Incoatec IμS microfocus source (Montel mirrors) at ambient conditions. The unit-cells, data reduction and absorption correction (multi-scan method) were conducted using CrysAlisPro[58] software package. The structure was solved by dual space direct methods SHELXT[59] and refinement by full-matrix least-squares against F2 using SHELX-2019/3.[60] All non-hydrogen atoms were refined anisotropically and hydrogen atoms were placed at calculated positions and refined in riding mode.

**Materials.** Acetonitrile (99.9 %, VWR), dichloromethane (99.9 %, stabilized with about 0.002 % of 2-methyl-2-butene, VWR), diethyl ether (99.9 %, VWR), ethanol absolute (99.9 %, VWR), acetone (99.9 %, VWR), ethylene glycol (≥99.5 %, Roth), methanol (99.9 %, VWR), n-hexane (97 %, VWR), dimethylformamide (99.9 %, VWR), ammonium hexafluorophosphate (99 %, Fluorochem), tetra-n-butylammonium hexafluorophosphate (≥98 %, TCI), ammonium chloride (>99 %, Acros Organics), aluminum oxide for chromatography (neutral, Brockmann I, 40–300 μm, 60 A, Thermo Fisher), silica gel for flash column chromatography (60 Å, 40–63 μm, ROCC), hydrochloric acid (37 %, VWR), sodium chloride (99.5 %, Acros Organics), 2-bromopyridine (99%, TCI), 4,4'-bipyridine (98%, across), n-Butyl lithium (2.5 M-hexane, Sigma-Aldrich), copper(II) chloride ($CuCl_2$) (99 %, across), rhenium(I) pentacarbonyl chloride ($Re(CO)_5Cl$) (99%, Sigma), 5-Boronoisophthalic acid (99%, BLDPharm), 2,4,6-triisopropylphenylboronic acid (99%, BLDPharm), 2,4,6-trimethylphenylboronic acid (99%, BLDPharm).1,1,1-trifluorethanol (99 %TCI), phenol (99%, TCI) tetra-*n*-butylammonium hexafluorophosphate (99 % electroanalysis, Sigma-Aldrich), deuterated acetonitrile (99.8 %D, Eurisotop), deuterated dimethylsulfoxide (99.8 %D, Eurisotop), were purchased from commercial suppliers and used as received. Water was purified by a Millipore Milli-Q system. [$Re^I$(bpy)$(CO)_3$Cl] was prepared according to a literature procedure.[3] Tetrakis(triphenylphosphine)palladium(0), [$Pd(P(C_6H_5)_3)_4$] ([$Pd(PPh_3)_4$]) was prepared following literature procedure[61] and stored in the dark at –20 °C. All reactions were conducted under inert atmosphere unless otherwise stated.

**Synthesis**

**6,6′-Dibromo-2,2′-bipyridine** This precursor was prepared according to a literature procedure with slight modifications.[62] Typical procedure involved using rigorously dried reagents and glassware. *n*-butyl lithium (2.5 M-hexane, 12.15 mL, 30.4 mmol, 1.2 equiv) was added over 1 hour to a –70 °C cooled suspension of 2,6-dibromopyridine (6.0 g, 25.3 mmol, 1 equiv) in anhydrous diethylether (24 mL) in a three-neck round bottom flask kept under argon. $CuCl_2$ (1.40 g, 15.7 mmol, 0.5 equiv) was then added and stirred for 30 minutes. The reaction mixture was thoroughly bubbled with dry air for 40 minutes. HCl (6 M, 60 mL) was subsequently slowly added to quench the reaction mixture that was then filtered and the solid product was washed with 0.5 M HCl. More product was obtained by extracting the filtrate with $CHCl_3$. The resulting combined brown solid was recrystallized from hot $CHCl_3$. The desired product was obtained as white crystals (2.37 g, 60 % yield) which were filtered off and washed with pentane. $^1$H NMR (400 MHz, $CDCl_3$, δ (ppm)): 8.39 – 8.34 (m, 2H), 7.66 (td, *J* = 7.8, 0.7 Hz, 2H), 7.49 (dd, *J* = 7.9, 0.9 Hz, 2H).

**6,6′-Dimesityl-2,2′-bipyridine ($bpy^{mes}$)** This was synthesized according to a literature procedure with slight modifications.[63] To a suspension of 6,6′-dibromo-2,2′-bipyridine (0.80 g, 2.54 mmol, 1 equiv) in toluene (170 mL), were added mesitylboronic acid, (1 g, 6.1 mmol, 2.4 equiv) and methanol (20 mL). Aqueous $Na_2CO_3$ (2 M, 32 mL) was then added, and the mixture was bubbled with argon for 10 minutes before adding [$Pd(PPh_3)_4$] (0.157 g, 0.127 mmol, 0.05 equiv). The reaction mixture was bubbled with argon for an additional 5 minutes before being refluxed for 72 h. Afterward, the reaction mixture was cooled to room temperature, the organic layer was taken and washed with saturated $Na_2CO_3$ solution (100 mL). The aqueous layer was washed with DCM (100 mL x 3 times) and the combined organic phases (toluene and DCM) were dried over anhydrous $MgSO_4$, filtered and evaporated under reduced pressure to obtain the title compound as a white solid (0.63 g, Yield 64%). $^1$H NMR: (300 MHz, $CDCl_3$, δ (ppm)): 8.38 (dd, *J* = 8.0, 1.1 Hz, 2H), 7.80 (t, *J* = 7.8 Hz, 2H), 7.21 (dd, *J* = 7.6, 1.1 Hz, 2H), 7.01 – 6.95 (m, 4H), 2.35 (s, 6H), 2.12 (s, 12H).

**6,6′- Di-(2,4,6-tiisopropylphenyl)-2,2′-bipyridine ($bpy^{trip}$).** To a suspension of 6,6′-dibromo-2,2′-bipyridyl (0.5 g, 1.59 mmol, 1 equiv) in toluene (170 mL), were added 2,4,6-triisopropylphenylboronic acid, (1.0 g, 4.03 mmol, 2.52 equiv) and methanol (7.5 mL). Aqueous $Na_2CO_3$ (2 M, 7.5 mL) was then added, and the mixture was bubbled with argon for 10 minutes before adding [$Pd(PPh_3)_4$] (0.100 g, 0.08 mol, 0.05 equiv). The reaction mixture was bubbled with argon for an additional 5 minutes before being refluxed for 72 h. Afterward, the reaction mixture was cooled to room temperature, the organic layer was taken and washed with saturated $Na_2CO_3$ solution (100 mL)). The aqueous layer of the reaction was washed with DCM (100 mL x 3 times) and the combined organic phases (toluene and DCM) were dried over anhydrous $MgSO_4$, filtered and evaporated under reduced pressure to obtain the title compound as a white solid (0.84 g, Yield 94%). $^1$H NMR (400 MHz, $CD_2Cl_2$, δ (ppm)): 8.41 (dd, *J* = 8.0, 1.1 Hz, 2H), 7.81 (t, *J* = 7.8 Hz, 2H), 7.26 (dd, *J* = 7.6, 1.1 Hz, 2H), 7.13 (s, 4H), 2.97 (p, *J* = 6.9 Hz, 2H), 2.68 – 2.54 (m, 4H), 1.32 (d, *J* = 6.9 Hz, 12H), 1.13 (dd, *J* = 7.9, 6.8 Hz, 24H). $^{13}$C NMR (400 MHz, $CD_2Cl_2$, δ (ppm)) δ 159.22, 155.67, 149.01, 146.59, 136.90, 136.57, 125.16, 120.73, 118.79, 34.53, 30.42, 24.00, 23.95, 23.86. HRMS m/z (calcd for [$bpy^{trip}$+H]$^+$ [$C_{40}H_{35}N_2$+H]$^+$ 561.4209, found 561.4221).

**6,6′-Di-(5-isophthalic acid)-2,2′-bipyridine ($bpy^{phth}$)** To a suspension of 6,6′-dibromo-2,2′-bipyridyl (0.80 g, 2.54 mmol, 1 equiv) and 5-boronoisophthalic acid (1.35 g, 6.42 mmol, 2.5 equiv) in methanol (12 mL), was added aqueous $Na_2CO_3$ (2 M, 12 mL) and the mixture was bubbled with argon for 10 minutes before adding [$Pd(PPh_3)_4$] (0.157 g, 0.127, 0.05 equiv). The reaction mixture was bubbled for an additional 5 minutes and refluxed for 72 h. Afterward, the reaction mixture was cooled to room temperature and the resulting white-brown solid was filtered, the solid was washed with 20 mL $H_2O$. The resultant aqueous phases were combined and acidified

with HCl (6 M) to pH ~ 2-3 to give a white precipitate which was filtered and washed with water, small portions of cold ethanol and diethylether and then dried under vacuum (0.64 g, Yield 56%). $^1$H NMR (400 MHz, $D_2O$/NaOD, δ (ppm)): 8.59 (d, *J* = 1.6 Hz, 4H), 8.44 (d, *J* = 7.8 Hz, 2H), 8.34 (t, *J* = 1.6 Hz, 2H), 8.10 (t, *J* = 7.8 Hz, 2H), 7.95 (d, *J* = 7.8 Hz, 2H). $^{13}$C NMR (400 MHz, d6-DMSO, δ (ppm)) δ 167.07, 155.60, 154.43, 139.97, 139.73, 132.65, 131.77, 131.03, 121.93, 120.63. HRMS m/z (calcd for $[M-H]^-$ $[C_{26}H_{15}N_2O_8- H]^-$ 483.0823, found 483.0828)

**[Re(bpy$^{mes}$)(CO)$_3$Cl] (2)** Pentacarbonylchlororhenium(I), $[ReCl(CO)_5]$ (100 mg, 0.276 mmol, 1equiv) and 6,6′-dimesityl-2,2′-bipyridine (bpy$^{mes}$) (108 mg, 0.276 mmol, 1 equiv) were suspended in toluene (15 mL) and refluxed at 120 °C for 24 h. After cooling to room temperature, the reaction mixture was filtered to remove any unreacted solid and the filtrate was reduced to 3 mL. Diethyl ether (10 mL) was then added and the solution was left for 2 hours to allow the precipitation of a yellow solid, which was filtered and washed with diethyl ether and dried in vacuum to afford a yellow product (125 mg, 65% Yield). $^1$H NMR (300 MHz, DMSO-$d_6$, δ (ppm)): 8.79 (dd, *J* = 8.4, 1.3 Hz, 2H), 8.33 (t, *J* = 7.9 Hz, 2H), 7.53 (dd, *J* = 7.7, 1.2 Hz, 2H), 7.29 – 7.09 (m, 2H), 6.97 (d, *J* = 7.3 Hz, 4H), 2.27 (s, 6H), 2.05 (s, 6H). HRMS m/z (calcd for $[M+Na]^+$ $[C_{31}H_{28}O_3N_2ClRe+Na]^+$ 719.12102, found 719.12152) and (calcd for $[M-Cl+MeCN]^+$ $[C_{33}H_{31}O_3N_3Re]^+$ 702.18895, found 702.18953)

**[Re(bpy$^{trip}$)(CO)$_3$Cl] (3)** Pentacarbonylchlororhenium(I), $[ReCl(CO)_5]$ (100 mg, 0.276 mmol, 1equiv) and di-(2,4,6-tiisopropylphenyl)-2,2′-bipyridine (bpy$^{trip}$) (108 mg, 0.276 mmol, 1 equiv) were suspended in toluene (15 mL) and refluxed at 120 °C for 24 h. After cooling to room temperature, the reaction mixture was filtered off, and the filtrate volume was reduced to 3 mL. Diethyl ether (10 mL) was added which resulted in the formation of a yellow precipitate that was collected by filtration, washed with diethyl ether and dried under vacuum to afford pure product. (170 mg, 71% Yield). $^1$H NMR (400 MHz, DMSO-$d_6$, δ (ppm)): 8.85 – 8.72 (m, 2H), 8.27 (t, *J* = 8.0 Hz, 2H), 7.73 (d, *J* = 6.8 Hz, 2H), 7.09 (d, *J* = 2.1 Hz, 4H), 2.97 – 2.80 (m, 2H), 2.44 (s, 4H), 1.28 – 1.10 (m, 24H), 0.91 (dd, *J* = 15.0, 6.8 Hz, 12H). $^{13}$C NMR (400 MHz, $CDCl_3$, δ (ppm)): 164.63, 158.08, 151.48, 147.08, 145.39, 136.83, 129.93, 122.75, 121.99, 120.89, 34.67, 30.90, 30.83, 25.73, 25.69, 24.06, 24.04, 23.34, 22.62. HRMS m/z (calcd for $[M+Na]^+$ $[C_{43}H_{52}O_3N_2{}^{35}ClRe+Na]^+$ 887.30882, found 887.30949) and (calcd for $[M-Cl+MeCN]^+$ $[C_{45}H_{55}O_3N_3Re]^+$ 870.37675, found 870.37766)

**[Re(bpy$^{phth}$)(CO)$_3$Cl] (4)** Pentacarbonylchlororhenium(I), $[ReCl(CO)_5]$ (100 mg, 0.276 mmol, 1 equiv) and 6,6′-di-(5-isophthalic acid)-2,2′-bipyridine (bpy$^{phth}$) (134 mg, 0.276 mmol, 1equiv) were suspended in methanol/toluene (1/1, 30 mL) mixture and heated at reflux for 96 h. The reaction mixture was concentrated to half its volume and filtered giving a yellow solid which was washed with diethylether (15 mL) and acetonitrile (10 mL). Subsequently, the solid was solubilized in MeOH/DMF mixture (1/0.2, 5 mL) which upon slow ether diffusion (10 mL) precipitated. The precipitate was filtered and washed with ether to afford a yellow solid (134 mg, 61 % Yield). $^1$H NMR (400 MHz, DMSO, δ (ppm)) δ 13.40 (s, 4H), 8.92 (d, *J* = 7.4 Hz, 2H), 8.60 (t, *J* = 1.6 Hz, 2H), 8.49 – 8.37 (m, 4H), 8.23 (s, 2H), 7.91 (dd, *J* = 7.7, 1.1 Hz, 2H), 7.28 – 7.08 (m, 6H). $^{13}$C NMR (400 MHz, DMSO-$d_6$, δ (ppm)) δ 166.59, 161.48, 158.11, 142.54, 141.12, 134.89, 133.83, 132.47, 132.10, 131.48, 128.36, 124.96, 118.64. HRMS m/z (calcd for $[M-Cl+MeCN]^+$ $[C_{31}H_{19}O_{11}N_3Re]^+$ 794.05437, found 794.05503)

## ASSOCIATED CONTENT

### Supporting Information

Additional experimental details, CCDC 2490565 (2), 2490566 (3), and 2447295 (4) include the supplementary crystallographic data and can be downloaded free of charge from The Cambridge Crystallographic Data Centre via www.ccdc.cam.ac.uk/structures. The Supporting Information is available free of charge on the ACS Publications website.

## AUTHOR INFORMATION

### Corresponding Author

Ludovic.Troian@uclouvain.be
abdullah.abudayyeh@uclouvain.be,

### Author Contributions

The manuscript was written through contributions of all authors. All authors have given approval to the final version of the manuscript.

### Funding Sources

Grant no. 40020332 (L.T.-G).

## ACKNOWLEDGMENT

This work was supported by the Fonds de la Recherche Scientifique (F.R.S.-FNRS) under grant CDR n°40020332. This publication benefited from the support of the Walloon Region as part of the financing of the FRFS-WEL-T strategic axis. L.T.-G. is a Chercheur Qualifié of the Fonds de la Recherche Scientifique – FNRS. A.A, S.D.K., K.R. B. E. and L.T.-G. gratefully acknowledge the UCLouvain for financial support. The work at Brookhaven National Laboratory (M.Z.E.) was carried out under contract DE-SC0012704 with the U.S. Department of Energy, Office of Science, Office of Basic Energy Sciences. A.L and S. G acknowledge the CERCA Program / Generalitat de Catalunya, and Severo Ochoa Excellence Accreditation CEX2024-001469-S funded by MCIU / AEI / 10.13039/501100011033. MICINN for PID2022-140143OB-I00 and Generalitat de Catalunya for the project 2021 SGR 01583.

## REFERENCES

1. Hughes, T. P.; Barnes, M. L.; Bellwood, D. R.; Cinner, J. E.; Cumming, G. S.; Jackson, J. B. C.; Kleypas, J.; van de Leemput, I. A.; Lough, J. M.; Morrison, T. H.*, et al.*, Coral Reefs in the Anthropocene. *Nature* **2017,** *546*, 82.

2. Johnstone, J. F.; Allen, C. D.; Franklin, J. F.; Frelich, L. E.; Harvey, B. J.; Higuera, P. E.; Mack, M. C.; Meentemeyer, R. K.; Metz, M. R.; Perry, G. L.*, et al.*, Changing Disturbance Regimes, Ecological Memory, and Forest Resilience. *Front. Ecol. Environ.* **2016,** *14*, 369-378.

3. Francke, R.; Schille, B.; Roemelt, M., Homogeneously Catalyzed Electroreduction of Carbon Dioxide—Methods, Mechanisms, and Catalysts. *Chem. Rev.* **2018,** *118*, 4631-4701.

4. Qiao, J.; Liu, Y.; Hong, F.; Zhang, J., A Review of Catalysts for the Electroreduction of Carbon Dioxide to Produce Low-Carbon Fuels. *Chem. Soc. Rev.* **2014,** *43*, 631-675.

5. Hawecker, J.; Lehn, J.-M.; Ziessel, R., Efficient Photochemical Reduction of Co₂ to Co by Visible Light Irradiation of Systems Containing Re(Bipy)(Co)3x or Ru(Bipy)32+–Co2+ Combinations as Homogeneous Catalysts. *J. Am. Chem. Soc.* **1983**, 536-538.

6. Hawecker, J.; Lehn, J.-M.; Ziessel, R., Electrocatalytic Reduction of Carbon Dioxide Mediated by Re(Bipy)(Co)3cl (Bipy = 2,2′-Bipyridine). *J. Chem. Soc., Chem. Commun.* **1984**, 328-330.

7. Costentin, C.; Drouet, S.; Robert, M.; Savéant, J.-M., A Local Proton Source Enhances Co2 Electroreduction to Co by a Molecular Fe Catalyst. *Science* **2012,** *338*, 90-94.

8. Rao, H.; Schmidt, L. C.; Bonin, J.; Robert, M., Visible-Light-Driven Methane Formation from Co(2) with a Molecular Iron Catalyst. *Nature* **2017,** *548*, 74-77.

9. Wang, M.; Torbensen, K.; Salvatore, D.; Ren, S.; Joulié, D.; Dumoulin, F.; Mendoza, D.; Lassalle-Kaiser, B.; Işci, U.; Berlinguette, C. P.*, et al.*, Co2 Electrochemical Catalytic Reduction with a Highly Active Cobalt Phthalocyanine. *Nat. Commun* **2019,** *10*, 3602.

10. Meshitsuka, S.; Ichikawa, M.; Tamaru, K., Electrocatalysis by Metal Phthalocyanines in the Reduction of Carbon Dioxide. *J. Chem. Soc. Chem. Comm.* **1974**, 158-159.

11. Lieber, C. M.; Lewis, N. S., Catalytic Reduction of Carbon Dioxide at Carbon Electrodes Modified with Cobalt Phthalocyanine. *J. Am. Chem. Soc.* **1984,** *106*, 5033-5034.

12. Guria, S.; Dolui, D.; Das, C.; Ghorai, S.; Vishal, V.; Maiti, D.; Lahiri, G. K.; Dutta, A., Energy-Efficient Co2/Co Interconversion by Homogeneous Copper-Based Molecular Catalysts. *Nature Comm.* **2023,** *14*, 6859.

13. Smieja, J. M.; Kubiak, C. P., Re(Bipy-Tbu)(Co)3cl−Improved Catalytic Activity for Reduction of Carbon Dioxide: Ir-Spectroelectrochemical and Mechanistic Studies. *Inorg. Chem.* **2010,** *49*, 9283-9289.

14. Guyot, M.; Lalloz, M.-N.; Aguirre-Araque, J. S.; Rogez, G.; Costentin, C.; Chardon-Noblat, S., Rhenium Carbonyl Molecular Catalysts for Co2 Electroreduction: Effects on Catalysis of Bipyridine Substituents Mimicking Anchorage Functions to Modify Electrodes. *Inorg. Chem.* **2022,** *61*, 16072-16080.

15. Sinha, S.; Berdichevsky, E. K.; Warren, J. J., Electrocatalytic Co2 Reduction Using Rhenium(I) Complexes with Modified 2-(2′-Pyridyl)Imidazole Ligands. *Inorg. Chim. Acta* **2017,** *460*, 63-68.

16. Garcia Osorio, D. A.; Neri, G.; Cowan, A. J., Hybrid Photocathodes for Carbon Dioxide Reduction: Interfaces for Charge Separation and Selective Catalysis. *ChemPhotoChem* **2021,** *5*, 595-610.

17. Windle, C. D.; Pastor, E.; Reynal, A.; Whitwood, A. C.; Vaynzof, Y.; Durrant, J. R.; Perutz, R. N.; Reisner, E., Improving the Photocatalytic Reduction of Co2 to Co through Immobilisation of a Molecular Re Catalyst on Tio2. *Chem-Eur. J.* **2015,** *21*, 3746-3754.

18. Schreier, M.; Luo, J.; Gao, P.; Moehl, T.; Mayer, M. T.; Grätzel, M., Covalent Immobilization of a Molecular Catalyst on Cu2o Photocathodes for Co2 Reduction. *J. Am. Chem. Soc.* **2016,** *138*, 1938-46.

19. Huang, J.; Xu, B.; Tian, L.; Pati, P. B.; Etman, A. S.; Sun, J.; Hammarström, L.; Tian, H., A Heavy Metal-Free Cuins2 Quantum Dot Sensitized Nio Photocathode with a Re Molecular Catalyst for Photoelectrochemical Co2 Reduction. *Chem. Commun.* **2019,** *55*, 7918-7921.

20. Jia, X.; Stewart-Jones, E.; Alvarez-Hernandez, J. L.; Bein, G. P.; Dempsey, J. L.; Donley, C. L.; Hazari, N.; Houck, M. N.; Li, M.; Mayer, J. M.*, et al.*, Photoelectrochemical Co2 Reduction to Co Enabled by a Molecular Catalyst Attached to High-Surface-Area Porous Silicon. *J. Am. Chem. Soc.* **2024,** *146*, 7998-8004.

21. Huffman, B. L.; Bein, G. P.; Atallah, H.; Donley, C. L.; Alameh, R. T.; Wheeler, J. P.; Durand, N.; Harvey, A. K.; Kessinger, M. C.; Chen, C. Y.*, et al.*, Surface Immobilization of a Re(I) Tricarbonyl Phenanthroline Complex to Si(111) through Sonochemical Hydrosilylation. *ACS Appl. Mater. Interfaces* **2023,** *15*, 984-996.

22. Müller, A. V.; Wierzba, W. M.; do Nascimento, L. G. A.; Concepcion, J. J.; Nikolaou, S.; Polyansky, D. E.; Polo, A. S., Tuning the Photocatalytic Co2 Reduction through Para-Substituents in Bipyridyl Rhenium Complexes. *Artificial Photosynthesis* **2025,** *xxx*, xxx.

23. Drover, M. W., A Guide to Secondary Coordination Sphere Editing. *Chem. Soc. Rev.* **2022,** *51*, 1861-1880.

24. Nyssen, N.; Abudayyeh, A.; Zhurkin, F.; Aoun, P.; Višnjevac, A.; Colasson, B.; Jabin, I.; Reinaud, O., Front Cover: Tmpa-Based Cavitary Cobalt (Ii) Funnel Complexes (Eur. J. Inorg. Chem. 22/2024). *Eur. J. Inorg. Chem.* **2024,** *27*, e202482201.

25. Rakowski DuBois, M.; DuBois, D. L., The Roles of the First and Second Coordination Spheres in the Design of Molecular Catalysts for H2 Production and Oxidation. *Chem. Soc. Rev.* **2009,** *38*, 62-72.

26. Matheu, R.; Ertem, M. Z.; Benet-Buchholz, J.; Coronado, E.; Batista, V. S.; Sala, X.; Llobet, A., Intramolecular Proton Transfer Boosts Water Oxidation Catalyzed by a Ru Complex. *J. Am. Chem. Soc.* **2015,** *137*, 10786-10795.

27. Azcarate, I.; Costentin, C.; Robert, M.; Savéant, J.-M., Through-Space Charge Interaction Substituent Effects in Molecular Catalysis Leading to the Design of the Most Efficient Catalyst of Co2-to-Co Electrochemical Conversion. *J. Am. Chem. Soc.* **2016,** *138*, 16639-16644.

28. Nichols, A. W.; Machan, C. W., Secondary-Sphere Effects in Molecular Electrocatalytic Co2 Reduction. *Front. Chem.* **2019,** *Volume 7 - 2019*.

29. Amanullah, S.; Gotico, P.; Sircoglou, M.; Leibl, W.; Llansola-Portoles, M. J.; Tibiletti, T.; Quaranta, A.; Halime, Z.; Aukauloo, A., Second Coordination Sphere Effect Shifts Co(2) to Co Reduction by Iron Porphyrin from Fe(0) to Fe(I). *Angew. Chem. Int. Ed. Engl.* **2024,** *63*, e202314439.

30. Matsubara, Y.; Shimojima, M.; Takagi, S., A Bi-Functional Second Coordination Sphere for Electrocatalytic Co2 Reduction: The Concerted Improvement by a Local Proton Source and Local Coulombic Interactions. *Chem. Lett.* **2019,** *49*, 315-317.

31. Sung, S.; Kumar, D.; Gil-Sepulcre, M.; Nippe, M., Electrocatalytic Co2 Reduction by Imidazolium-Functionalized Molecular Catalysts. *J. Am. Chem. Soc.* **2017,** *139*, 13993-13996.

32. Rotundo, L.; Garino, C.; Priola, E.; Sassone, D.; Rao, H.; Ma, B.; Robert, M.; Fiedler, J.; Gobetto, R.; Nervi, C., Electrochemical and Photochemical Reduction of Co2 Catalyzed by Re(I) Complexes Carrying Local Proton Sources. *Organometallics* **2019,** *38*, 1351-1360.

33. Haviv, E.; Azaiza-Dabbah, D.; Carmieli, R.; Avram, L.; Martin, J. M. L.; Neumann, R., A Thiourea Tether in the Second Coordination Sphere as a Binding Site for Co2 and a Proton Donor Promotes the Electrochemical Reduction of Co2 to Co Catalyzed by a Rhenium Bipyridine-Type Complex. *J. Am. Chem. Soc.* **2018,** *140*, 12451-12456.

34. Talukdar, K.; Sinha Roy, S.; Amatya, E.; Sleeper, E. A.; Le Magueres, P.; Jurss, J. W., Enhanced Electrochemical Co2 Reduction by a Series of Molecular Rhenium Catalysts Decorated with Second-Sphere Hydrogen-Bond Donors. *Inorg. Chem.* **2020,** *59*, 6087-6099.

35. Chen, K.-H.; Wang, N.; Yang, Z.-W.; Xia, S.-M.; He, L.-N., Tuning of Ionic Second Coordination Sphere in Evolved Rhenium Catalyst for Efficient Visible-Light-Driven Co2 Reduction. *ChemSusChem* **2020,** *13*, 6284-6289.

36. Roell, S. A.; Schrage, B. R.; Ziegler, C. J.; White, T. A., Isolating Substituent Effects in Re(I)-Phenanthroline Electrocatalysts for Co2 Reduction. *Inorg. Chim. Acta* **2020,** *503*, 119397.

37. Elsby, M. R.; Kumar, A.; Daniels, L. M.; Ertem, M. Z.; Hazari, N.; Mercado, B. Q.; Paulus, A. H., Linear Free Energy Relationships Associated with Hydride Transfer from [(6,6′-R2-Bpy)Re(Co)3h]: A Cautionary Tale in Identifying Hydrogen Bonding Effects in the Secondary Coordination Sphere. *Inorg. Chem.* **2024,** *63*, 19396-19407.

38. Wrighton, M.; Morse, D. L., Nature of the Lowest Excited State in Tricarbonylchloro-1,10-Phenanthrolinerhenium(I) and Related Complexes. *J. Am. Chem. Soc.* **1974,** *96*, 998-1003.

39. Kjellberg, M.; Ohleier, A.; Thuéry, P.; Nicolas, E.; Anthore-Dalion, L.; Cantat, T., Photocatalytic Deoxygenation of N–O Bonds with Rhenium Complexes: From the Reduction of Nitrous Oxide to Pyridine N-Oxides. *Chem. Sci.* **2021,** *12*, 10266-10272.

40. Worl, L. A.; Duesing, R.; Chen, P.; Ciana, L. D.; Meyer, T. J., Photophysical Properties of Polypyridyl Carbonyl Complexes of Rhenium(I). *Dalton Trans.* **1991**, 849-858.

41. Thomas, K. R. J.; Lin, J. T.; Lin, H.-M.; Chang, C.-P.; Chuen, C.-H., Ruthenium and Rhenium Complexes of Fluorene-Based Bipyridine Ligands: Synthesis, Spectra, and Electrochemistry. *Organometallics* **2001,** *20*, 557-563.

42. Evans, R. C.; Douglas, P.; Winscom, C. J., Coordination Complexes Exhibiting Room-Temperature Phosphorescence: Evaluation of Their Suitability as Triplet Emitters in Organic Light Emitting Diodes. *Coord. Chem. Rev.* **2006,** *250*, 2093-2126.

43. Troian-Gautier, L.; Turlington, M. D.; Wehlin, S. A. M.; Maurer, A. B.; Brady, M. D.; Swords, W. B.; Meyer, G. J., Halide Photoredox Chemistry. *Chem. Rev.* **2019,** *119*, 4628-4683.

44. Clark, M. L.; Cheung, P. L.; Lessio, M.; Carter, E. A.; Kubiak, C. P., Kinetic and Mechanistic Effects of Bipyridine (Bpy) Substituent, Labile Ligand, and Brønsted Acid on Electrocatalytic Co2 Reduction by Re(Bpy) Complexes. *ACS Catal.* **2018,** *8*, 2021-2029.

45. Sullivan, B. P.; Bolinger, C. M.; Conrad, D.; Vining, W. J.; Meyer, T. J., One- and Two-Electron Pathways in the Electrocatalytic Reduction of Co2 by Fac-Re(Bpy)(Co)3cl (Bpy = 2,2′-Bipyridine). *J. Chem. Soc., Chem. Commun.* **1985**, 1414-1416.

46. Elgrishi, N.; Rountree, K. J.; McCarthy, B. D.; Rountree, E. S.; Eisenhart, T. T.; Dempsey, J. L., A Practical Beginner's Guide to Cyclic Voltammetry. *J. Chem. Ed.* **2018,** *95*, 197-206.

47. Zanello, P., *Inorganic Electrochemistry: Theory, Practice and Application*. Royal Society of Chemistry: Cambridge, UK, 2003; p 615.

48. Nie, W.; McCrory, C., Electrocatalytic $Co_2$ Reduction by a Cobalt Bis(Pyridylmonoimine) Complex: Effect of Acid Concentration on Catalyst Activity and Stability. *Chem. Commun.* **2018,** *54*, 1579-1582.

49. Bordwell, F. G., Equilibrium Acidities in Dimethyl Sulfoxide Solution. *Acc. Chem. Res.* **1988,** *21*, 456-463.

50. Stuardi, F. M.; Tiozzo, A.; Rotundo, L.; Leclaire, J.; Gobetto, R.; Nervi, C., Efficient Electrochemical Reduction of Co2 to Formate in Methanol Solutions by Mn-Functionalized Electrodes in the Presence of Amines. *Chem-Eur. J.* **2022,** *28*, e202104377.

51. Sampson, M. D.; Nguyen, A. D.; Grice, K. A.; Moore, C. E.; Rheingold, A. L.; Kubiak, C. P., Manganese Catalysts with Bulky Bipyridine Ligands for the Electrocatalytic Reduction of Carbon Dioxide: Eliminating Dimerization and Altering Catalysis. *J. Am. Chem. Soc.* **2014,** *136*, 5460-5471.

52. Appel, A. M.; Helm, M. L., Determining the Overpotential for a Molecular Electrocatalyst. *ACS Catal.* **2014,** *4*, 630-633.

53. Yu, H. S.; He, X.; Li, S. L.; Truhlar, D. G., Mn15: A Kohn–Sham Global-Hybrid Exchange–Correlation Density Functional with Broad Accuracy for Multi-Reference and Single-Reference Systems and Noncovalent Interactions. *Chem. Sci.* **2016,** *7*, 5032-5051.

54. Marenich, A. V.; Cramer, C. J.; Truhlar, D. G., Universal Solvation Model Based on Solute Electron Density and on a Continuum Model of the Solvent Defined by the Bulk Dielectric Constant and Atomic Surface Tensions. *J. Phys. Chem. B* **2009,** *113*, 6378-6396.

55. Weigend, F.; Ahlrichs, R., Balanced Basis Sets of Split Valence, Triple Zeta Valence and Quadruple Zeta Valence Quality for H to Rn: Design and Assessment of Accuracy. *Phys. Chem. Chem. Phys.* **2005,** *7*, 3297-3305.

56. Frisch, M.; Trucks, G.; Schlegel, H.; Scuseria, G.; Robb, M.; Cheeseman, J.; Scalmani, G.; Barone, V.; Petersson, G.; Nakatsuji, H., Gaussian 16 Revision C. 01, 2016. *Gaussian Inc. Wallingford CT* **2016,** *1*, 572.

57. Cramer, C. J., *Essentials of Computational Chemistry*. John Wiley & Sons: 2004; p 1–624.

58. Sheldrick, G. M., Crystal Structure Refinement with Shelxl. *Acta Cryst. C* **2015,** *71*, 3-8.

59. Sheldrick, G. M., Shelxt - Integrated Space-Group and Crystal-Structure Determination. *Acta Cryst.* **2015,** *71*, 3-8.

60. CrysAlis, C., Crysalis Red. *Rigaku Oxford Diffraction* **2008**.

61. Coulson, D. R.; Satek, L. C.; Grim, S. O., Tetrakis(Triphenylphosphine)Palladium(0). In *Inorganic Syntheses*, McGraw-Hill, Inc: 1972; pp 121-124.

62. Shimada, H.; Sakurai, T.; Kitamura, Y.; Matsuura, H.; Ihara, T., Metallo-Regulation of the Bimolecular Triplex Formation of a Peptide Nucleic Acid. *Dalton Trans.* **2013,** *42*, 16006-16013.

63. Benson, E. E.; Rheingold, A. L.; Kubiak, C. P., Synthesis and Characterization of 6,6′-(2,4,6-Triisopropylphenyl)-2,2′-Bipyridine (Tripbipy) and Its Complexes of the Late First Row Transition Metals. *Inorg. Chem.* **2010,** *49*, 1458-1464.

Insert Table of Contents artwork here

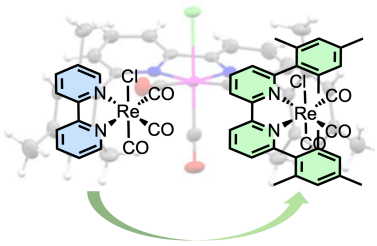


Second Coordination Sphere
Selective $CO_2$-to-CO conversion
Faradaic efficiency > 97%